Topological Subspace-Induced Bound State in the Continuum

Yi-Xin Xiao, Guancong Ma, Zhao-Qing Zhang, and C. T. Chan*
Department of Physics and Institute for Advanced Study, Hong Kong University of Science and Technology, Clear Water Bay, Kowloon, Hong Kong, China
(Received 11 December 2016; published 17 April 2017)

We propose and experimentally realize a new kind of bound states in the continuum (BICs) in a class of systems constructed by coupling multiple identical one-dimensional chains, each with inversion symmetry. In such systems, a specific separation of the Hilbert space into a topological and a nontopological subspace exists. Bulk-boundary correspondence in the topological subspace guarantees the existence of a localized interface state which can lie in the continuum of extended states in the nontopological subspace, forming a BIC. Such a topological BIC is observed experimentally in a system consisting of coupled acoustic resonators.

DOI: 10.1103/PhysRevLett.118.166803

Bound states in the continuum (BICs) are spatially confined modes that coexist with a continuous spectrum of extended states [1,2]. BICs were first proposed using custom-made potentials which are hard to realize. Recently, several mechanisms of forming BICs have been proposed such as parameter fine-tuning [3–8], space symmetry incompatibility [9–16], separations of coordinate variables [17], chiral symmetry [18–20], inverse construction [21,22], and PT symmetry [23]. BICs have been experimentally demonstrated in optical waveguides [6,9,19,20,22], atoms [7], and photonic crystal slabs [4,24]. Recently, trapped light has been observed within the radiation continuum in photonic crystal slabs [4], and its robustness was explained in terms of topological charges [25]. Because of their high-Q nature, BICs can be used for low-threshold lasing, chemical sensing, and narrow-band filtering [2].

Recently, topological matters have attracted a lot of attention in condensed matter [26,27] and cold atoms [28,29]. Promising application of topological matters and related concepts can be found from classical wave systems [30–37] to noise-robust quantum computation [38–46]. We find a new mechanism to form a BIC based on the concept of topological subspaces. We will construct a system in which the Hilbert space can be partitioned into a topological and a nontopological subspace, and a topological interface state due to bulk-boundary correspondence of the topological subspace can coexist with the continuum of the nontopological subspace, forming a BIC.

We will show that there exists a class of quasi-one-dimensional (1D) periodic systems in which nontopological bands coexist with topological bands characterized by quantized Zak phases. The Zak phase [34,47] is a geometric phase used to characterize the bulk topology of 1D systems, and it has quantized values (0 or π) when the system has inversion symmetry. We consider a class of systems constructed by coupling multiple identical 1D chains, each with inversion symmetry. The interchain couplings remove the inversion symmetry in the entire system. Consequently, the Zak phase of each band is, in general, not quantized. However, we show that certain interchain couplings allow the Hilbert space of the whole system to be separated into a nontopological and a topological subspace. In the topological subspace, bulk-boundary correspondence assures the existence of a spatially confined midgap state occurring at the interface between two topologically different phases. This confined state can be used to create a BIC if its energy overlaps with the continuum of the nontopological modes. The new mechanism for BICs we propose here is very general, robust, and simple to realize, due to its topological essence. We experimentally implement the idea by using 1D phononic crystals (PCs) consisting of coupled acoustic resonators and demonstrate the existence of a topological BIC.

Model.—We start by considering two identical Su-Schrieffer-Heeger (SSH) chains [48] coupled indirectly through another chain as shown in Fig. 1(a). There are five "atoms" in a unit cell, which are labeled by numbers 1–5. The labels t and s denote the intracell and intercell hoppings, and β is the hopping between two adjacent 5th sites. r_1 and r_2 denote the interchain couplings. The on-site energies are assumed to be ϵ_5 for the 5th site and 0 for all the other sites. We take $\beta = 0$ at first without a loss of generality. We set the lattice constant $a = 1$ as the unit of length.

In momentum space, the Hamiltonian has the form

$$\mathcal{H}(k) = \begin{pmatrix} 0 & W & 0 & 0 & r_1 \\ W^* & 0 & 0 & 0 & 0 \\ 0 & 0 & 0 & W & r_2 \\ 0 & 0 & W^* & 0 & 0 \\ r_1 & 0 & r_2 & 0 & \epsilon_5 \end{pmatrix}, \quad (1)$$

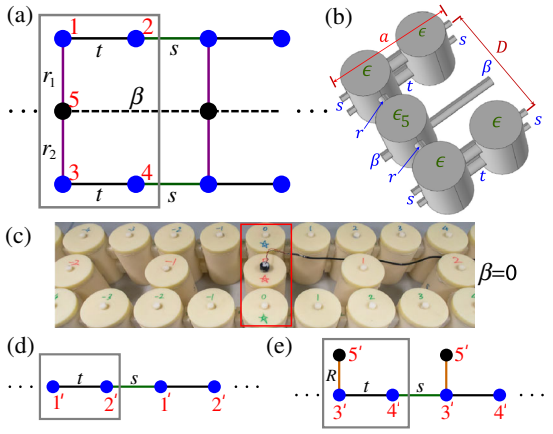

FIG. 1. (a) Two identical SSH chains coupled by a coupler atom per unit cell. The hopping parameters and indices of the atom orbitals are labeled. The on-site energies are $\epsilon_1 = \epsilon_2 = \epsilon_3 = \epsilon_4 = 0$ and ϵ_5. (b) A unit cell consisting of coupled acoustic cavities. (c) Photos of the coupled acoustic cavities with $\beta = 0$ for the measurement of the topological interface state in the midgap. The regions encircled by a red rectangle are the interface. (d) and (e) show the virtual lattices in the topological and the nontopological subspace, respectively.

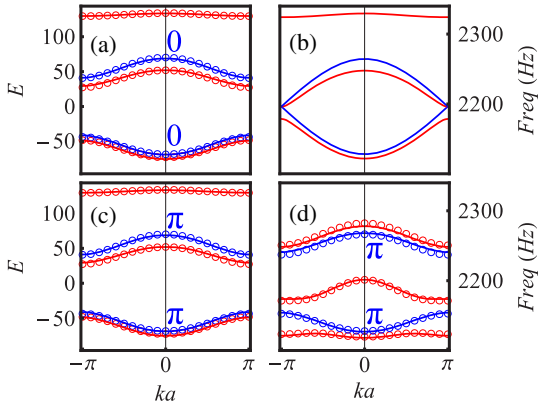

FIG. 2. Solid curves (left y axis) in (a)–(c) show the band inversion and quantized Zak phases for the 2nd and 4th bands (blue) when hopping parameters are changed from (a) $|t| > |s|$ with $t = -55.7$, $s = -13.6$, through (b) the transition point with $t = s = -34$, to (c) $|t| < |s|$ with $t = -13.6$, $s = -55.7$. Zak phases for the three bands labeled by red are not quantized. The same values are chosen for other parameters with $\epsilon_5 = 110.2, \beta = 0$, and $r_1 = r_2 = -33.7$. (d) Solid curves show the band structure with parameters $t = -13.6$, $s = -56.9$, $r_1 = r_2 = -26.5$, $\epsilon_5 = -22$, and $\beta = 13.5$. All the parameters above are obtained by fitting to COMSOL calculated bands marked by circles (right y axis).

where $W = t + se^{-ik}$. In the absence of interchain couplings, namely, $r_1 = r_2 = 0$, the system has two doubly degenerate SSH bands with $E_\pm(k) = \pm\sqrt{t^2 + s^2 + 2ts\cos k}$, which have quantized Zak phases as required by the existence of inversion symmetry in each chain, and a flat band $E = \epsilon_5$. The presence of interchain couplings lifts the degeneracy and breaks the inversion symmetry of the system, and the prediction of quantized Zak phases does not apply [47]. The absence of inversion symmetry can be observed more easily by arranging all the sites onto a 1D configuration [49]. The band structures for three typical situations are shown by solid lines in Figs. 2(a)–2(c): (a) $|t| > |s|$; (b) $|t| = |s|$; (c) $|t| < |s|$. We calculate the Zak phase according to $\theta = i\oint dk\langle u(k)|\partial_k u(k)\rangle$, where $|u(k)\rangle$ is the eigenstate of $\mathcal{H}(k)$. We find that the Zak phases are not quantized for the three bands shown by red curves. However, two bands in Figs. 2(a) and 2(c) shown by blue curves still possess quantized Zak phases of 0 and π even though the system has no inversion center. The separation of quantized and nonquantized bands becomes more transparent if we block-diagonalize $\mathcal{H}(k)$ by using $U^{-1}\mathcal{H}(k)U = \mathcal{H}^{\mathrm{BD}}(k)$, where

$$\mathcal{H}^{\mathrm{BD}}(k) = \begin{pmatrix} 0 & W & 0 & 0 & 0 \\ W^* & 0 & 0 & 0 & 0 \\ 0 & 0 & 0 & W & R \\ 0 & 0 & W^* & 0 & 0 \\ 0 & 0 & R & 0 & \epsilon_5 \end{pmatrix}, \tag{2}$$

$$U = \frac{1}{R}\begin{pmatrix} -r_2 & 0 & r_1 & 0 & 0 \\ 0 & -r_2 & 0 & r_1 & 0 \\ r_1 & 0 & r_2 & 0 & 0 \\ 0 & r_1 & 0 & r_2 & 0 \\ 0 & 0 & 0 & 0 & R \end{pmatrix}, \tag{3}$$

and $R = \sqrt{r_1^2 + r_2^2}$. It is interesting to point out that the two quantized blue bands shown in Figs. 2(a) and 2(c) have the SSH dispersions $E = E_\pm(k)$, which come from the upper 2×2 block. As these two bands have quantized Zak phases, the associated subspace can be considered "topological." We emphasize that the existence of a topological subspace holds for arbitrary values of r_1 and r_2. The lower 3×3 block represents the nontopological subspace. The survival of a set of SSH bands in the presence of r_1 and r_2 is due to the fact that identical SSH chains outnumber the coupling channels [49]. Thus, the block-diagonalization explicitly separates the Hilbert space into a topological and a nontopological subspace. The closing of the gap between two blue bands at $|t| = |s|$ in Fig. 2(b) implies a topological phase transition in the topological subspace.

The existence of quantized Zak phases in the topological subspace implies a hidden symmetry. The unitary matrix U transforms the basis of old "orbitals" $|i\rangle$ to a new one, i.e., $|i'\rangle = \sum_{j=1}^{5} U_{ji}|j\rangle$, where $i = 1, 2, 3, 4, 5$. Explicitly, the basis for the 2×2 SSH block in Eq. (2) are two "superorbitals,"

$$|1'\rangle = (-r_2|1\rangle + r_1|3\rangle)/R,$$
$$|2'\rangle = (-r_2|2\rangle + r_1|4\rangle)/R, \tag{4}$$

where $\langle i'|j'\rangle = \delta_{ij}$, $i, j = 1, 2$, and δ_{ij} is the Kronecker delta function. The hidden symmetry [49] becomes evident if we consider the subsystem as a virtual SSH model with each unit cell comprising two superorbitals $|1'\rangle$ and $|2'\rangle$, as shown in Fig. 1(d) [49]. The virtual lattice explicitly possesses inversion symmetry, leading to quantized Zak phases for the associated two blue bands. For comparison, the virtual lattice corresponding to the 3×3 block in Eq. (2) is also shown in Fig. 1(e), which possesses no inversion symmetry; therefore, the Zak phases for the associated three red bands are not quantized [49].

Equation (4) reveals that the wave functions in the topological subspace vanish on the 5th sites and are antisymmetric between two SSH chains if $r_1 = r_2$. These special properties will be used to experimentally differentiate a topological interface mode from nontopological modes.

Realization of the tight-binding model.—The tight-binding model can be realized using coupled acoustic resonators. The unit cell is shown in Fig. 1(b). We choose a dipole mode of a cylindrical cavity to represent the "orbitals" [49]. The cavities are made of hard plastics and filled with air. They all have the same radius of 3 cm. The height of the interchain cavity 5 is treated as a tuning parameter, whereas the height for the rest is 8.0 cm. Hoppings among the cavities are facilitated by small connecting tubes, with radii $R_t = 9$ mm, $R_s = 4$ mm, and $R_r = 6$ mm for hoppings t, s, and r, respectively. For simplicity, we choose $r_1 = r_2 = r$. In this special case, the wave functions in the topological and nontopological subspace are odd and even, respectively, but we note that the topological or nontopological states do not have parity symmetry in the general case. The lattice constant is $a = 16$ cm, and the interchain distance is $D = 15$ cm. The separation between two neighboring cavities on an SSH chain is $a/2$. With these parameters, we compute the band structure using COMSOL. The band structures for the case of $\beta = 0$ are shown in Figs. 2(a) and 2(c) by circles, where the eigenfrequency is shown on the right vertical axis. The band structures from the tight-binding fitting are shown on the left vertical axis by the solid curves in Figs. 2(a) and 2(c). The excellent agreement shows that our coupled acoustic cavities can be faithfully described by the tight-binding model.

Topological interface mode.—We first demonstrate the existence of a topological interface state due to bulk-boundary correspondence in the topological subspace. We use the unit cell with $\beta = 0$ to construct an interface as shown in Fig. 3(a). A fabricated sample is shown in Fig. 1(c), in which the left PC has Zak phase 0 while the right one has Zak phase π, joining at the interface by two weak bonds. The height of middle cavities is 7.6 cm. The topological interface state is numerically identified at $f = 2187$ Hz in the eigenspectrum and shown by a blue dot in Fig. 3(b). In fact, there is another localized state inside the gap at $f = 2173$ Hz (red dot) which has even parity and

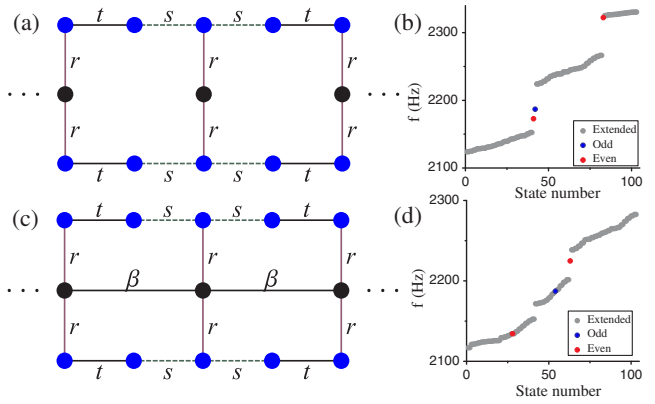

FIG. 3. Interface structures and their eigenspectra for $\beta = 0$ [(a) and (b)] and $\beta \neq 0$ [(c) and (d)]. There are three sites at the interface and ten cells on each side in (a) and (c). The odd (even) interface modes are marked by blue (red) dots in (c) and (d). The topological (odd) interface mode is inside the gap in (c) and inside the continuum in (d).

comes from the nontopological subspace [49]. Actually, there is a second nontopological interface state marked by the upper red dot in Fig. 3(b), which is not of interest here [49].

In the experiment, we excite the states in the topological and nontopological subspace by antiphase and in-phase excitations, respectively. The topological interface mode is selectively excited experimentally at 2186 Hz by an antiphase excitation, which decays exponentially away from the interface. It has odd parity and very small amplitudes in the middle cavities, 2 orders of magnitude smaller than those on the two SSH chains. Using an in-phase excitation, another nontopological interface mode is also identified experimentally at 2173 Hz, which has even parity and has significant amplitudes in the middle cavities. The detailed results are shown in Sec. G of Supplemental Material.

Topological BIC.—We next show that a BIC can be constructed by embedding the topological interface state in a continuous spectrum of extended states in the nontopological subspace. This can happen if the nontopological band between two SSH bands overlaps with the topological interface state. To realize this, we change the height of the middle cavities to 8.1 cm and connect the neighboring middle cavities with small tubes of radius $R_\beta = 6$mm. This newly added connection brings a hopping $\beta = 13.5$ and changes the (5, 5) matrix element in Eqs. (1) and (2) from ϵ_5 to $\epsilon_5 + 2\beta \cos k$. Thus, the separation of Hilbert space as well as the existence of SSH bands remains intact. Now the 3rd nontopological band lies in the middle of two SSH bands, as shown in Fig. 2(d).

The interface is constructed according to Fig. 3(c), and a fabricated sample is shown in Fig. S1 [49]. As shown in Fig. 3(d), the topological interface state marked by the blue dot is clearly embedded in the continuum of the middle

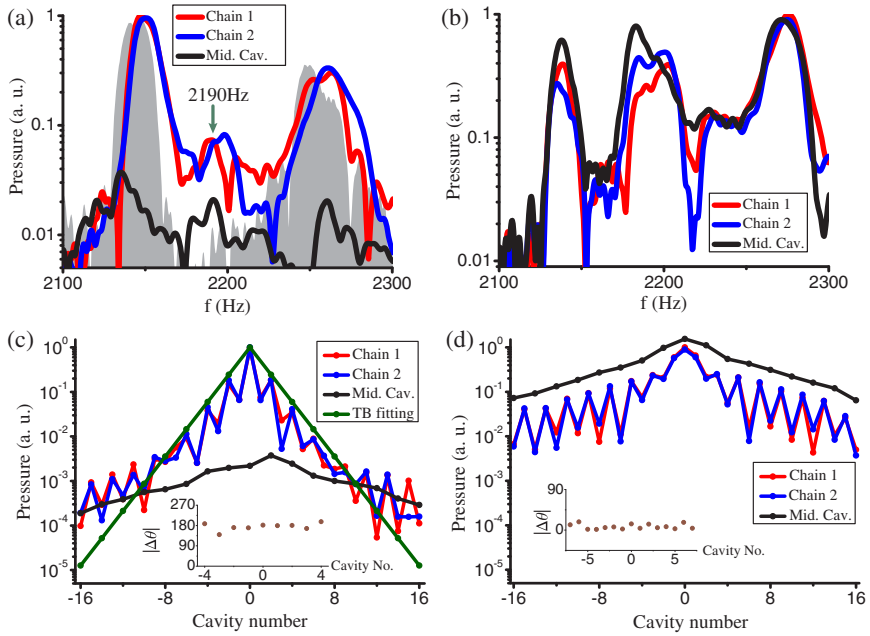

FIG. 4. (a),(b) The response spectra with an (a) antiphase and (b) an in-phase excitation. The green arrow in (a) marks the topological BIC at 2190 Hz. The gray shaded region in (a) denotes the pressure response without an interface. (c),(d) The field distributions of the (c) odd interface state and (d) the even extended state at 2190 Hz. The green line in (c) shows the tight-binding fitting result. The insets in (c) and (d) show the phase difference of pressure responses on the two SSH chains, which demonstrates the odd and the even parity of the excited modes, respectively.

nontopological band and is therefore a BIC. Experimentally, we separately excite the states in the topological and nontopological subspaces using antiphase and in-phase sources, respectively. This is achieved by placing two antiphase or in-phase loudspeakers on the two SSH chains at the seventh unit cell away from the interface. The pressure response is measured at the interface. The spectral responses to antiphase and in-phase excitations are shown in Figs. 4(a) and 4(b) in log scale, respectively. In Fig. 4(a), we show the pressure measured on the two SSH chains (blue and red curves). For comparison, we also measured the pressure response of a periodic structure with ten unit cells using an antiphase excitation and showed the profile of the pressure response by the gray shaded region in Fig. 4(a). The band gap at about 2200 Hz is clearly demonstrated for the periodic structure. The small peak marked by a green arrow at 2190 Hz on the red curve inside the band gap (2175–2230 Hz) unambiguously shows the BIC. In addition, the response at the middle cavity is much smaller than those on the SSH chains. In Fig. 4(b), in the same spectral range near 2200 Hz, we see a pronounced band of high pressure responses instead of a band gap. Also, the pressure in the middle cavity is on a par with or even exceeds that on the SSH chains. We measured the pressure amplitudes of each site so as to clearly demonstrate that they are localized at the BIC frequency 2190 Hz. We used both antiphase and in-phase excitations by exciting the system at the PC interface. Figure 4(c) shows the antiphase field profile, indicating the exponential decay of the pressure on the two SSH chains away from the interface (blue and red) with the decay constant matching well with the analytic tight-binding result $|\ln(s/t)|^{-1}$ [49] for the topological zero energy interface mode (green). Agreeing with the theoretical prediction, the field amplitude in the middle cavities is much smaller. Under the in-phase excitation, we see in Fig. 4(d) that the field amplitudes are of the same magnitude for both SSH chains and the middle cavities. The fields are extended across the system with a much smaller decay constant compared to the antiphase situation. This small decay is due to dissipation. In the insets in Figs. 4(c) and 4(d), the phase differences $|\Delta\theta| = |\theta_1 - \theta_2|$ between the two SSH chains are shown, which demonstrate the parity of the excited modes. The combination of Figs. 4(c) and 4(d) confirms the eigenspectrum shown in Fig. 3(d) and shows clearly the existence of a topological bound state in a nontopological continuum.

In summary, we theoretically and experimentally demonstrated a topological BIC, attributed to the separation of the Hilbert space into a topological subspace and a nontopological one. We emphasize that the topological BIC actually exists for any pair of unequal r_1 and r_2 in which the system does not have any obvious symmetries [49] and also in generalized models with multiple chains and next-nearest-neighbor hoppings [49]. The topological subspace-induced BIC can also be implemented in cold atoms in deep lattices [28,29] and optical systems such as weakly coupled optical waveguide arrays [9,19,20] and high dielectric photonic crystals where the tight-binding description holds. The concept of a topological subspace

and BICs may also be useful to other communities such as quantum computation [38–40].

We thank Kam Tuen Law, Shubo Wang, Meng Xiao, and Ruoyang Zhang for helpful discussions. G. M. thanks Zhiyu Yang for equipment and Xiaonan Zhang and Yue Xiao for helping with sample fabrication. This work is supported by Research Grants Council Hong Kong (AoE/P-02/12).

Y. X. and G. M. contributed equally to this work.

*Corresponding author.
phchan@ust.hk

[1] J. von Neuman and E. Wigner, Phys. Z. **30**, 465 (1929).
[2] C. W. Hsu, B. Zhen, A. D. Stone, J. D. Joannopoulos, and M. Soljačić, Nat. Rev. Mater. **1**, 16048 (2016).
[3] H. Friedrich and D. Wintgen, Phys. Rev. A **32**, 3231 (1985).
[4] C. W. Hsu, B. Zhen, J. Lee, S.-L. Chua, S. G. Johnson, J. D. Joannopoulos, and M. Soljačić, Nature (London) **499**, 188 (2013).
[5] D. C. Marinica, A. G. Borisov, and S. V. Shabanov, Phys. Rev. Lett. **100**, 183902 (2008).
[6] S. Weimann, Y. Xu, R. Keil, A. E. Miroshnichenko, A. Tünnermann, S. Nolte, A. A. Sukhorukov, A. Szameit, and Y. S. Kivshar, Phys. Rev. Lett. **111**, 240403 (2013).
[7] J. Neukammer, H. Rinneberg, G. Jönsson, W. E. Cooke, H. Hieronymus, A. König, K. Vietzke, and H. Spinger-Bolk, Phys. Rev. Lett. **55**, 1979 (1985).
[8] F. Monticone and A. Alù, Phys. Rev. Lett. **112**, 213903 (2014).
[9] Y. Plotnik, O. Peleg, F. Dreisow, M. Heinrich, S. Nolte, A. Szameit, and M. Segev, Phys. Rev. Lett. **107**, 183901 (2011).
[10] N. Moiseyev, Phys. Rev. Lett. **102**, 167404 (2009).
[11] L. S. Cederbaum, R. S. Friedman, V. M. Ryaboy, and N. Moiseyev, Phys. Rev. Lett. **90**, 013001 (2003).
[12] E. N. Bulgakov and A. F. Sadreev, Phys. Rev. B **78**, 075105 (2008).
[13] M. Callan, C. M. Linton, and D. V. Evans, J. Fluid Mech. **229**, 51 (1991).
[14] S. P. Shipman and S. Venakides, Phys. Rev. E **71**, 026611 (2005).
[15] R. L. Schult, H. W. Wyld, and D. G. Ravenhall, Phys. Rev. B **41**, 12760 (1990).
[16] M. Robnik, J. Phys. A **19**, 3845 (1986).
[17] N. Rivera, C. W. Hsu, B. Zhen, H. Buljan, J. D. Joannopoulos, and M. Soljačić, Sci. Rep. **6**, 33394 (2016).
[18] J. Mur-Petit and R. A. Molina, Phys. Rev. B **90**, 035434 (2014).
[19] R. A. Vicencio, C. Cantillano, L. Morales-Inostroza, B. Real, C. Mejía-Cortés, S. Weimann, A. Szameit, and M. I. Molina, Phys. Rev. Lett. **114**, 245503 (2015).
[20] S. Mukherjee, A. Spracklen, D. Choudhury, N. Goldman, P. Öhberg, E. Andersson, and R. R. Thomson, Phys. Rev. Lett. **114**, 245504 (2015).
[21] M. I. Molina, A. E. Miroshnichenko, and Y. S. Kivshar, Phys. Rev. Lett. **108**, 070401 (2012).
[22] G. Corrielli, G. Della Valle, A. Crespi, R. Osellame, and S. Longhi, Phys. Rev. Lett. **111**, 220403 (2013).
[23] M. I. Molina and Y. S. Kivshar, Stud. Appl. Math. **133**, 337 (2014).
[24] J. Lee, B. Zhen, S.-L. Chua, W. Qiu, J. D. Joannopoulos, M. Soljačić, and O. Shapira, Phys. Rev. Lett. **109**, 067401 (2012).
[25] B. Zhen, C. W. Hsu, L. Lu, A. D. Stone, and M. Soljačić, Phys. Rev. Lett. **113**, 257401 (2014).
[26] M. Z. Hasan and C. L. Kane, Rev. Mod. Phys. **82**, 3045 (2010).
[27] X.-L. Qi and S.-C. Zhang, Rev. Mod. Phys. **83**, 1057 (2011).
[28] N. Goldman, G. Juzeliūnas, P. Öhberg, and I. B. Spielman, Rep. Prog. Phys. **77**, 126401 (2014).
[29] N. R. Cooper, Adv. Phys. **57**, 539 (2008).
[30] F. D. M. Haldane and S. Raghu, Phys. Rev. Lett. **100**, 013904 (2008).
[31] Z. Wang, Y. D. Chong, J. D. Joannopoulos, and M. Soljačić, Phys. Rev. Lett. **100**, 013905 (2008).
[32] M. Hafezi, E. A. Demler, M. D. Lukin, and J. M. Taylor, Nat. Phys. **7**, 907 (2011).
[33] L. Lu, J. D. Joannopoulos, and M. Soljačić, Nat. Photonics **8**, 821 (2014).
[34] M. Xiao, G. Ma, Z. Yang, P. Sheng, Z. Q. Zhang, and C. T. Chan, Nat. Phys. **11**, 240 (2015).
[35] E. Prodan and C. Prodan, Phys. Rev. Lett. **103**, 248101 (2009).
[36] C. L. Kane and T. C. Lubensky, Nat. Phys. **10**, 39 (2014).
[37] S. Weimann, M. Kremer, Y. Plotnik, Y. Lumer, S. Nolte, K. G. Makris, M. Segev, M. C. Rechtsman, and A. Szameit, Nat. Mater. **16**, 433 (2016).
[38] A. Kitaev, Ann. Phys. (N.Y.) **303**, 2 (2003).
[39] P. Milman and R. Mosseri, Phys. Rev. Lett. **90**, 230403 (2003).
[40] C. E. R. Souza, J. A. O. Huguenin, P. Milman, and A. Z. Khoury, Phys. Rev. Lett. **99**, 160401 (2007).
[41] J. Du, J. Zhu, M. Shi, X. Peng, and D. Suter, Phys. Rev. A **76**, 042121 (2007).
[42] L. E. Oxman and A. Z. Khoury, Phys. Rev. Lett. **106**, 240503 (2011).
[43] M. Johansson, M. Ericsson, K. Singh, E. Sjöqvist, and M. S. Williamson, Phys. Rev. A **85**, 032112 (2012).
[44] A. Z. Khoury, L. E. Oxman, B. Marques, A. Matoso, and S. Pádua, Phys. Rev. A **87**, 042113 (2013).
[45] A. Z. Khoury and L. E. Oxman, Phys. Rev. A **89**, 032106 (2014).
[46] A. A. Matoso, X. Sánchez-Lozano, W. M. Pimenta, P. Machado, B. Marques, F. Sciarrino, L. E. Oxman, A. Z. Khoury, and S. Pádua, Phys. Rev. A **94**, 052305 (2016).
[47] J. Zak, Phys. Rev. Lett. **62**, 2747 (1989).
[48] W. P. Su, J. R. Schrieffer, and A. J. Heeger, Phys. Rev. Lett. **42**, 1698 (1979).
[49] See Supplemental Material at http://link.aps.org/supplemental/10.1103/PhysRevLett.118.166803 for discussions on symmetry, bulk-boundary correspondence and generalizations, which includes Refs [50–52].
[50] C. D. Meyer, *Matrix Analysis and Applied Linear Algebra* (Society for Industrial and Applied Mathematics, Philadelphia, 2000).
[51] M. Inui, S. A. Trugman, and E. Abrahams, Phys. Rev. B **49**, 3190 (1994).
[52] B. Sutherland, Phys. Rev. B **34**, 5208 (1986).